Journal of Materials Chemistry A

ROYAL SOCIETY OF CHEMISTRY

PAPER

Cite this: *J. Mater. Chem. A*, 2024, **12**, 3954

Electrochemically and chemically stable electrolyte–electrode interfaces for lithium iron phosphate all-solid-state batteries with sulfide electrolytes†

Tenglong Lu, [ab] Sheng Meng *[abc] and Miao Liu *[acd]

Received 13th October 2023
Accepted 4th January 2024

DOI: 10.1039/d3ta06227a

rsc.li/materials-a

All-solid-state batteries which use inorganic solid materials as electrolytes are the futuristic energy storage technology because of their high energy density and improved safety. One of the significant challenges facing all-solid-state batteries is the poor compatibility between electrolyte and electrode materials at their point of contact, which negatively impacts battery performance. Therefore, it is important to find appropriate interfacial materials that can mediate the electrolyte–electrode reaction while maintaining efficient ionic transportation in all-solid-state batteries. In the past, the mechanism of interaction between the electrolyte and the electrode was explored and a number of potential coating materials for layered NCM and $LiCoO_2$ cathodes were found. In this paper, employing a similar computational scheme, we extend such coating material screening to $LiFePO_4$-based all-solid-state batteries with sulfide electrolytes. Harnessing a trove of first-principles data in the *Atomly* materials database, we comprehensively evaluated and screened the coating compounds based on their thermodynamic stability, (electro)chemical stability, electronic conductance, ionic conductance, *etc.*, and successfully found 41 promising coating compounds out of the 54 005 candidates. This paper offers insightful directives for optimizing the performance of $LiFePO_4$-based all-solid-state batteries.

1. Introduction

Lithium iron phosphate (chemical formula $LiFePO_4$, shortened as LFP) has emerged as a crucial energy material for electric vehicles (EVs) owing to its commendable cycle stability, cost-effectiveness, environmental friendliness, and impressive gravimetric capacity.[1] Nonetheless, commercial LFP batteries utilizing liquid electrolytes are plagued by inherent issues, such as iron dissolution, flammability concerns, and restricted electrochemical stability.[2] To address these challenges, the development of all-solid-state batteries (ASSBs) based on LFP holds significant promise.

The most significant challenge in the transition from liquid electrolytes (LEs) to solid-state electrolytes (SSEs) lies in searching for solid-state phases that can offer Li-ion conductivities at least comparable to those of LEs (~10 mS cm^{-1}). Fortunately, to date, several innovative Li-ion solid-state conductors have been identified, primarily classified into oxide- and sulfide-based chemistries.[3–6] Experimentally, Yan *et al.* assembled an LFP-based ASSB with the $Li_7La_3Zr_2O_{12}$ (LLZO) electrolyte.[7] However, owing to the relatively modest Li-ion conductivity of LLZO (~10^{-1} mS cm^{-1}), the thickness of the electrolyte should be reduced to just a few micrometers. This results in a thin-film ASSB with limited capacity, which poses a challenge for its application in EVs. Compared to oxides, sulfide-based SSEs can achieve significantly improved Li-ion conductivities, typically two orders of magnitude higher.[4] Surprisingly, several sulfide electrolytes exhibit superior Li-ion conductivities, even surpassing those of LEs, such as $Li_{10}GeP_2S_{12}$ (~12 mS cm^{-1}),[3] glass-ceramic $Li_7P_3S_{11}$ (~17 mS cm^{-1}),[8] and $Li_{9.54}Si_{1.74}P_{1.44}S_{11.7}Cl_{0.3}$ (~25 mS cm^{-1}).[6] Therefore, it is expected that large-sized LFP-based ASSBs incorporating sulfide electrolytes will be promising next-generation energy storage devices.

Despite the breakthrough in Li-ion superionic conductors, solid-state interfaces (SEIs) have been detected at the SSE/cathode contact points, resulting in high interfacial impedance and irreversible capacity fading upon cycling.[9] The presence of SEIs can be attributed to two main reasons: (1) the instability of the SSE at high or low lithium chemical potential,

[a]*Beijing National Laboratory for Condensed Matter Physics, Institute of Physics, Chinese Academy of Sciences, Beijing 100190, China. E-mail: smeng@iphy.ac.cn; mliu@iphy.ac.cn*

[b]*School of Physical Sciences, University of Chinese Academy of Sciences, Beijing 100190, China*

[c]*Songshan Lake Materials Laboratory, Dongguan, Guangdong 523808, China*

[d]*Center of Materials Science and Optoelectronics Engineering, University of Chinese Academy of Sciences, Beijing 100049, China*

† Electronic supplementary information (ESI) available. See DOI: https://doi.org/10.1039/d3ta06227a

which induces the electrochemical decomposition of the SSE, and (2) the favorable chemical reactivity between the SSE and the electrode. To mitigate the deleterious side reaction at the SSE/electrode interface, one of the most effective strategies is to apply a buffer layer on the electrode to prevent direct contact between the active material and the electrolyte.

In this study, we systematically evaluated viable compounds that could serve as promising coating layers between the LFP cathode and sulfide-based SSEs to prevent any deleterious (electro)chemical reactions. Previously, a number of papers have investigated the same issues for layered compounds and developed screening protocols. For example, Zhu *et al.* demonstrated that Li_3TaO_4 and Li_5TaO_5 can effectively protect the interface between $Li_7La_3Zr_2O_{12}$ and $LiCoO_2$.[10] Xiao *et al.* identified several lithium phosphates such as LiH_2PO_4, $LiTi_2(PO_4)_3$, and $LiPO_3$ as interfacial coatings for the NCM-Li_3PS_4 system.[11] LFP batteries have become one of the most successful commercial cathodes. However, based on our knowledge, comprehensive screening of coating materials for LFP electrodes has not been conducted, and this paper aims to fill this gap. Leveraging a dataset of 54 005 lithium-containing compounds from the *Atomly* materials database,[12,13] we conducted a systematic assessment of their thermodynamic stability, band gap, electrochemical stability window, chemical reactivity, and ionic migration barrier. Finally, forty-one screened compounds were identified as appealing coating materials for LFP-based ASSBs with sulfide electrolytes. Additionally, by performing a statistical analysis of the reactivity between different pairs of chemical compositions, we proposed several rules of thumb that can offer effective guidance for coating selection in different electrode–electrolyte systems.

2. Methods

2.1 First-principles density functional theory calculations

Density functional theory (DFT) calculations were performed using the projector-augmented wave (PAW) method implemented in the Vienna *ab initio* simulation package (VASP).[14,15] A plane wave energy cutoff of 520 eV and a *k*-point grid of $n_{\text{kpoints}} \times n_{\text{atoms}}$ >1000 were adopted for all the calculations. The calculations relied on the Perdew–Burke–Ernzerhof (PBE) generalized gradient approximation (GGA) exchange-correlation functional.[16] Additional setting details can be found in our previous studies.[17–21] All the energy data and band gaps were directly extracted from the *Atomly* materials database.[18]

2.2 Atomly database

The *Atomly* materials database (URL: atomly.net (**http://atomly.net**)) is a comprehensive repository of inorganic crystalline compounds, housing the DFT calculated properties of approximately 349 000 materials. These valuable data encompass essential information such as optimized structures, energy band, density of states, elasticity, and thermodynamic stability. The dataset was meticulously developed through high-throughput DFT runs, utilizing a protocol akin to the one used in the Materials Project. As such, these data are compatible with the Materials Project, adding significant depth to the overall available dataset as it is currently 2.3 times larger. Notably, Atomly features an abundance of newly added structures, primarily composed of transition metal-containing ionic compounds. These structures have been created through element substitution and then screened for their thermodynamic stability by an AI model. Consequently, the dataset is particularly well-suited for electrochemical applications.

2.3 Phase diagram constructions

To evaluate the thermodynamic stability of compounds, phase diagrams were constructed based on the energy data in *Atomly* materials database. The python materials genomics (*pymatgen*) open-source library was employed to generate all the phase diagrams.[22]

2.4 Electrochemical stability window

The calculation of the electrochemical stability window employed the method developed in several pioneer studies.[10,23] For a composition c, we convert its energy $E[c]$ to a grand potential $\Phi[c]$, assuming that the system is open to lithium

$$\Phi[c,\mu_{\text{Li}}] = E[c] - n_{\text{Li}}[c]\mu_{\text{Li}} \quad (1)$$

where $n_{\text{Li}}[c]$ is the lithium concentration in the compound, and μ_{Li} denotes the lithium chemical potential determined by the external environment. For each μ_{Li}, we constructed a grand potential phase diagram for the composition c, from which the corresponding grand potential convex hull can be derived. By varying μ_{Li}, there exists a chemical potential range, $[\mu_{\text{red}},\mu_{\text{ox}}]$, within which the composition c is located precisely on the grand potential convex hull. μ_{red} and μ_{ox} denote the reduction and oxidation onset for the composition c, respectively. Finally, the electrochemical stability window, $[V_{\text{red}},V_{\text{ox}}]$, can be derived from the chemical potential range based on the Nernst equation:

$$V_{\text{red}} = \frac{\mu^0_{\text{Li}} - \mu_{\text{red}}}{e} \quad (2)$$

$$V_{\text{ox}} = \frac{\mu^0_{\text{Li}} - \mu_{\text{ox}}}{e} \quad (3)$$

where μ^0_{Li} stands for the chemical potential for lithium metal and e is the elementary charge.

2.5 Interfacial chemical reaction energy

According to the relative methodology developed by recent studies,[10,23] we performed calculations of the interfacial chemical reaction to evaluate the contact compatibility between two materials. An interface consisting of two compositions, c_a and c_b, exhibits a composition of

$$c_{\text{interface}}[c_a,c_b,x] = xc_a + (1-x)c_b \quad (4)$$

where x denotes the molar fraction of the composition c_a which varies from 0 to 1. Omitting the surface energy, this interface shows an energy of

$$E_{\text{interface}} = E_{\text{gs}}[c_{\text{interface}}] \quad (5)$$

where $E_{\text{gs}}[c_{\text{interface}}]$ is the ground-state energy at the composition $c_{\text{interface}}$ derived from the corresponding energy convex hull. Finally, the interfacial chemical reaction energy between c_a and c_b is

$$\Delta E_{\text{rxt}} = \min_{x\in[0,1]} \left\{ E_{\text{gs}}[xc_a + (1-x)c_b] - xE[c_a] - (1-x)E[c_b] \right\} \quad (6)$$

To assess the interfacial reaction energy at an applied voltage, the voltage V can be converted to the lithium chemical potential μ_{Li} based on the Nernst equation. Using eqn (1), all the energies mentioned in eqn (6) can be replaced with the corresponding grand potentials:

$$\Delta\Phi_{\text{rxt},\mu_{\text{Li}}} = \min_{x\in[0,1]} \left\{ \begin{array}{l} \phi_{\text{gs},\mu_{\text{Li}}}[xc_a + (1-x)c_b] - \\ x\phi_{\mu_{\text{Li}}}[c_a] - (1-x)\phi_{\mu_{\text{Li}}}[c_b] \end{array} \right\} \quad (7)$$

2.6 Migration barrier calculations

Coarse migration barrier evaluation was performed using the bond-valence approach, as implemented in the *SoftBV* package.[24] Furthermore, the accurate migration barriers of Li-ion vacancies were evaluated using the climbing image nudged elastic band (NEB) method.[25,26] The GGA functional was adopted. A reciprocal space discretization of 25 k-points per Å^{-1} was applied, and the convergence criteria were set as 1×10^{-5} eV for electronic steps and 0.05 eV Å^{-1} for ionic steps. For each compound examined in this work, all its distinct vacancy migration paths were assessed using NEB, and the highest barrier was chosen as the net migration barrier.

3. Results

3.1 Incompatibility between sulfide-based SSEs and the LFP cathode

Previous experimental and theoretical research efforts have primarily focused on addressing interfacial issues between SSEs and high-voltage cathode materials.[11,27–30] Herein, we initially conduct a comprehensive evaluation of the interfacial compatibility between the sulfide-based SSE and the LFP cathode, considering both electrochemical and chemical perspectives. Several outstanding sulfide electrolytes were considered for the evaluation, including LiChT-type Li_4SnS_4 (LSnS),[31] iodide-based $Li_7P_2S_8I$ (LPSI),[32] argyrodite Li_6PS_5Cl (LPSC),[33] halide-rich argyrodite $Li_{5.5}PS_{4.5}Cl_{1.5}$ ($L_{5.5}$PSC),[34] β-Li_3PS_4 (LPS),[35] glass-ceramic $Li_7P_3S_{11}$ (L_7PS),[8] $Li_{10}GeP_2S_{12}$ (LGPS),[3] thio-LISICON $Li_{3.25}Ge_{0.25}P_{0.75}S_4$ ($L_{3.25}$GPS),[36] LGPS-type $Li_{9.54}Si_{1.74}P_{1.44}S_{11.7}Cl_{0.3}$ (LSiPSC),[6] and $Li_{9.6}P_3S_{12}$ ($L_{9.6}$PS).[6]

As depicted in Fig. 1a, all the sulfide-based electrolytes demonstrate rather narrow electrochemical stability windows, typically ranging from 1.7 to 2.2 V, which is consistent with previous experimental and theoretical observations.[10] For instance, Cronk *et al.* conducted linear sweep voltammetry to confirm that the electrochemical window of argyrodite LPSC ranges from 1.4 to 2.3 V.[37] This finding aligns closely with our predicted range of 1.7–2.1 V, indicating the accuracy of our calculation results. The dashed line in Fig. 1a illustrates the equilibrium voltage of LFP upon cycling, corresponding to the potential of the Fe^{2+}/Fe^{3+} redox couple. It is evident that there are significant gaps between the oxidation limits of sulfide-based SSEs (~2.2 V) and the operating voltage of LFP (~3.45 V), implying that sulfide-based SSEs could potentially undergo significant electrochemical oxidation when in direct contact with the LFP active materials upon cycling. For instance, at 3.45 V, LGPS will be dramatically oxidized to

$$Li_{10}GeP_2S_{12} \rightarrow Li + GeS_{14} + P_2S_7 + GeS_2 \quad (8)$$

with a low electrochemical decomposition energy of −744 meV per atom. These sluggish Li-ion conductors may be deposited on the surface of LFP particles, leading to poor cycling performance and reduced capacity retention. Besides, commonly used electron conductive materials in LFP cathode composites, such as carbon additives, have the potential to significantly accelerate this electrochemical oxidation process. Hence, we predicted that sulfide-based SSEs would demonstrate poor electrochemical compatibility with the LFP cathode.

Additionally, we estimated the chemical reactivity of sulfide-based SSEs toward cathode materials. Both LFP and $FePO_4$ (FP) were considered, corresponding to the discharged and charged states of the battery, respectively. As demonstrated in Fig. 1b, all the sulfide electrolytes undergo favorable reactions with LFP, exhibiting an average reaction energy of −150 meV per atom. These reactions are thermodynamically driven by the formation of lower-energy equilibrium phases, primarily composed of iron sulfides and lithium phosphates. For example, argyrodite LPSC mixed with LFP favors a reaction of

$$L_6PS_5Cl + LiFePO_4 \rightarrow Li_3PO_4 + Li_4P_2O_7 + FePS + FeS_2 + LiCl \quad (9)$$

with a decomposition energy of −153 meV per atom. The generated iron sulfides, such as FeS_2 and FeS, possess moderate-to-high electronic conductivities, which might not efficiently passivate LFP active materials, enabling the continued electrochemical oxidation of sulfide electrolytes. In the case of a charged state (the second column in Fig. 1b), even more pronounced reactions may take place between the electrolytes and FP, delivering an average decomposition energy of −230 meV per atom. Hence, it is evident that sulfide-based SSEs are likely to exhibit strong chemical reactivity with both the LFP and FP active materials.

Finally, we evaluated the reactivity of the SSE/cathode interface across the entire operating voltage range of the LFP electrode. As depicted in Fig. 1c, due to a combination of electrochemical and chemical reactivity, all the interfaces between sulfide electrolytes and LFP demonstrate very poor stability, with reaction energies ranging from ~−230 meV per atom at 2 V

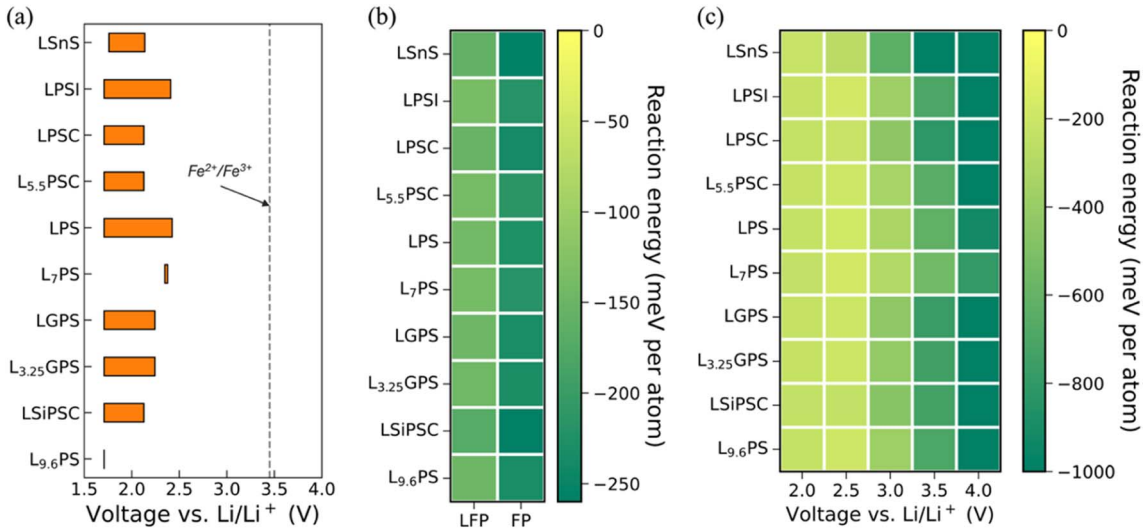

Fig. 1 (a) Electrochemical stability windows of various sulfide-based SSEs. (b) Chemical reactivity of sulfide-based SSEs with LFP and FP. (c) Interfacial reactivity between sulfide-based SSEs and LFP at voltages ranging from 2–4 V.

to over −1000 meV per atom at 4 V. It was demonstrated that the interfacial issues between the SSE and cathode would become extremely challenging at an applied voltage. For instance, the aforementioned LPSC/LFP interface undergoes chemical decomposition, delivering a reaction energy of −153 meV per atom. Whereas, at merely a low operating voltage of 2.5 V, the reactivity between LPSC and LFP is greatly enhanced, boosting the reaction energy to −218 meV per atom. The details of sulfide electrolyte decomposition at applied voltages and the reactions between electrolytes and electrodes can be found in Tables S1–S3, ESI.†

Overall, sulfide-based SSEs exhibit poor compatibility with LFP cathode materials. Strong side reactions will take place at the SSE/cathode interface, leading to the gradual deterioration of the LFP cathode and a decline in battery performance. To mitigate this interfacial issue, one of the most effective strategies is to coat a buffer layer between the LFP active materials and sulfide-based SSE.

3.2 Preliminary screening of coating candidates for the LFP cathode

Fig. 2 depicts a schematic representation of a high-throughput workflow for screening potential coating candidates for the LFP cathode. Lithium-free binary compounds such as Al_2O_3, ZrO_2, and AlF_3 are commonly employed as coating layers in batteries with liquid electrolytes.[38,39] However, these kinds of materials are generally poor Li-ion conductors. It has been demonstrated that maintaining a high Li-ion conductivity at the interfaces between battery components is critical for achieving good performance in ASSBs. Hence, as the initial screening criteria, we concentrated on the 54 005 lithium-containing compounds available in the *Atomly* materials database.

For each compound, an energy convex hull is constructed in the corresponding phase space, and the derived energy above the hull (E_{hull}) is employed as a quantitative metric to evaluate its thermodynamic stability. A material with $E_{hull} = 0$ lies on the convex hull and is a thermodynamically stable phase at 0 K. Whereas for a compound with $E_{hull} > 0$, there is a thermodynamic driving force for its decomposition, and it is a metastable (or unstable) phase. To take into account potential kinetic stabilization, we set a stability criterion of $E_{hull} \leq 5$ meV per atom to identify synthesizable materials. To mitigate the electrochemical oxidation of sulfide-based SSEs, coating layers should effectively passivate the surface of LFP particles. Hence, we set a band-gap (E_g) criterion of $E_g \geq 0.5$ eV to screen compounds with potentially low electronic conductivities. These two screening criteria returned a total of 3196 materials.

An effective coating layer should possess a sufficiently wide electrochemical stability window to prevent it from being reduced at the SSE side or oxidized at the cathode side.[40] As

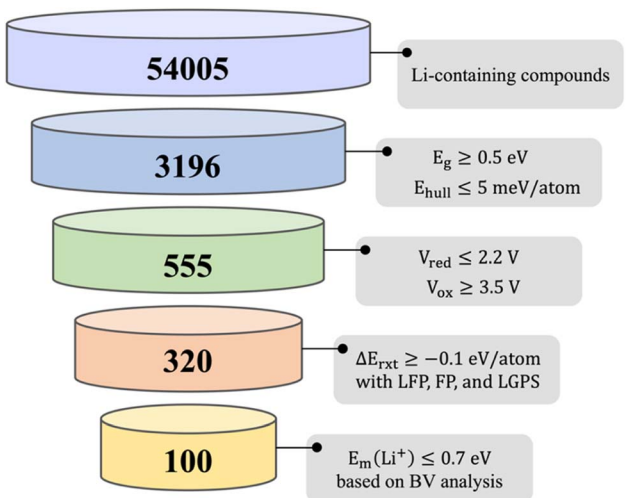

Fig. 2 A screening workflow for potential coating candidates for the LFP cathode.

described earlier in Section 3.1, sulfide-based SSEs demonstrate an average electrochemical oxidation limit of ~2.2 V, and the operating voltage of LFP is ~3.5 V. Hence, the electrochemical stability window of a coating layer should at least range from 2.2 to 3.5 V, corresponding to a reduction limit (V_{red}) of lower than 2.2 V, and an oxidation limit (V_{ox}) of higher than 3.5 V. This electrochemical stability screening further reduced the list to 555 materials.

When a cathode is coated with a buffer layer, two new interfaces are introduced: the coating/SSE interface and the coating/cathode interface. Low chemical reactivity is essential to ensure that these interfaces are intact. In this context, LGPS was selected as a representative compound for sulfide-based SSEs. We computed the reaction energies (ΔE_{rxt}) for the coating/LGPS, coating/LFP, and coating/FP interfaces. A threshold value of −100 meV per atom was employed to identify compounds that possess moderate-to-excellent chemical compatibility with all three interfaces. This chemical stability screening cut the compound list down to 320 materials.

While the number of compounds has been significantly reduced from 54 005 to 320, it remains computationally expensive to assess the dynamic properties of all these materials using *ab initio* methods. Hence, we performed a bond-valence (BV) evaluation to calculate their net Li-ion migration barriers (E_m) with a relatively low computational cost. A criterion of $E_m \leq 0.7$ eV was set to exclude compounds with poor Li-ion conductivities. Finally, this migration barrier screening popped up 100 materials. We will delve into a detailed discussion of these coating candidates in the subsequent sections.

3.3 In-depth investigation of coating candidates for the LFP cathode

We categorized these 100 coating candidates into six groups based on their anionic chemistries, which include non-polyanionic oxides, fluorides, phosphates, borates, silicates, and others (oxyfluorides and chlorides).

3.3.1 Non-polyanionic oxides. Fig. 3 illustrates both the electrochemical stability windows (Fig. 3a) and the interfacial compatibility (Fig. 3b) of the 12 non-polyanionic (NP) oxide coating candidates. To date, several lithium ternary metal oxides have been extensively employed as cathode coatings, including $LiAlO_2$,[41] $LiTaO_3$,[42] Li_2ZrO_3,[43] $Li_4Ti_5O_{12}$,[44] and $LiNbO_3$.[45] However, only $LiAlO_2$ and $Li_4Ti_5O_{12}$ are included in our preliminary screening results. According to the BV analysis, $LiTaO_3$ was screened out because of its high net Li-ion migration barrier, which is consistent with the experimental observations. For Li_2ZrO_3, deleterious chemical side reactions may take place at the Li_2ZrO_3/FP interface with a ΔE_{rxt} of −124 meV per atom. Besides, $LiNbO_3$ is predicted to undergo a favorable reaction with LGPS, delivering a ΔE_{rxt} of −108 meV per atom.

As depicted in Fig. 3b, driven by a great tendency of breaking P–S bonds to form $(PO_4)^{3-}$ polyanionic units, the majority of the screened NP oxides demonstrate non-negligible chemical reactivity with LGPS. Only $LiAlO_2$ and $LiAl_2H_6BrO_6$ possess exceptional compatibility with LGPS, with a $|\Delta E_{rxt}|$ of smaller than 20 meV per atom. Li_2CO_3 has been frequently employed as the cathode coating layer in ASSBs with sulfide electrolytes. However, we predicted a favorable reactivity between Li_2CO_3 and LGPS, following the reaction of

$$Li_2CO_3 + Li_{10}GeP_2S_{12} \rightarrow CS_{14} + Li_4GeS_4 + Li_2S + Li_3PO_4 + C \quad (10)$$

with a ΔE_{rxt} of −78 meV per atom. Due to the generation of carbon, Li_2CO_3 cannot passivate the surface of the cathode after decomposition, leading to the continuing electrochemical oxidation of LGPS. Experimentally, a Li_2CO_3/$LiNbO_3$ hybrid coating has been deposited on the surface of NCM622 in an argyrodite-based ASSB (Li_2CO_3 and $LiNbO_3$ exhibit similar reaction energies and decomposition products to argyrodite LPSC and LGPS).[46] Regarding the cycling performance of the battery, it presents a steady capacity decay, ultimately resulting in a capacity retention rate of only ~56% after 200 cycles. In

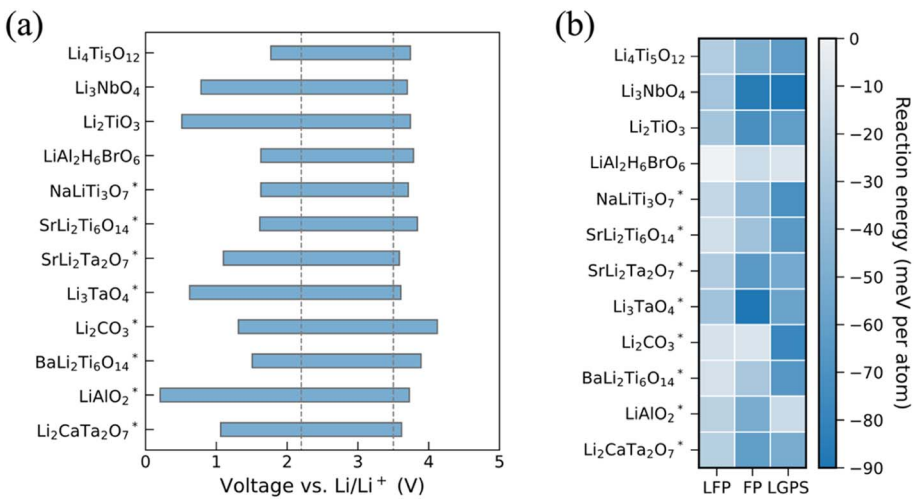

Fig. 3 (a) Electrochemical stability windows of various NP oxides. (b) Chemical reactivity of NP oxides with LFP, FP, and LGPS. Compounds marked with a star denote their experimental existence.

contrast, an ASSB consisting of a β-LPS electrolyte and an $LiAlO_2$-coated NCM111 cathode exhibits a capacity retention rate of ~75% after 400 cycles.[47] Compared to Li_2CO_3 and $LiNbO_3$, $LiAlO_2$ demonstrates more promising coating performance, which could be attributed to its excellent chemical compatibility with sulfide-based SSEs.

Similarly, as shown in Fig. 3b, there are strong driving forces for these NP oxides to react with LFP or FP as well. Even $LiAlO_2$ exhibits a non-trivial reactivity with FP ($\Delta E_{rxt} = -51$ meV per atom), making it less applicable in an LFP-based battery. To understand the poor chemical compatibility between NP oxides and LFP/FP, we conducted a statistical analysis of the interfacial reactivity between lithium ternary metal oxides and different cathode materials, including $LiCoO_2$ (LCO), $Li_{0.5}CoO_2$ ($L_{0.5}CO$), $LiNiO_2$ (LNO), $Li_{0.5}NiO_2$ ($L_{0.5}NO$), LFP, and FP. As depicted in Fig. 4, compared to LCO and LNO cathodes, lithium ternary metal oxides notably demonstrate poor compatibility with LFP and FP, with an average $|\Delta E_{rxt}|$ of greater than 100 meV per atom. This phenomenon is induced by a great tendency for these metal oxides to react with phosphorus-containing compounds to form the lower-energy Li_3PO_4 phase. In short, NP oxides may not be well-suited for coating LFP cathodes in ASSBs with sulfide electrolytes.

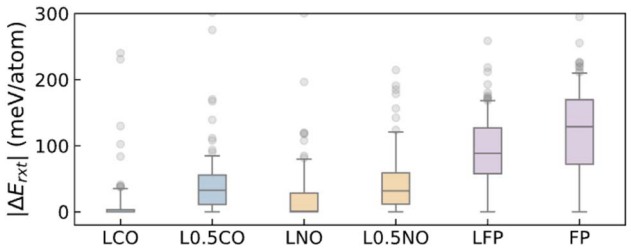

Fig. 4 Chemical reactivity of lithium ternary oxides with LCO, L0.5CO, LNO, L0.5NO, LFP, and FP. Each box represents the quartiles of the dataset (gray dots), and the whisker extends to show the rest of the distribution.

3.3.2 Fluorides. Presently, fluorides have not been utilized as coatings for cathode active materials in ASSBs. Our screening workflow returned 30 lithium fluorides for coating LFP cathodes in ASSBs with sulfide electrolytes. As depicted in Fig. 5a, these lithium fluorides demonstrate very wide electrochemical stability windows, with oxidation limits exceeding 5 V. The remarkable oxidation resistances of fluorides can be attributed to their deep hybrid orbitals, originating from the high electronegativity of fluorine. $LiAlF_4$, Li_2TiF_6, and Li_2ZrF_6 have been used to coat high-voltage cathode active materials in batteries with liquid electrolytes.[48–50] However, only Li_2TiF_6 is involved in our screening results. According to the *Atomly* materials database, $LiAlF_4$ shows a relatively large metastability with an E_{hull} of 45 meV per atom. Besides, Li_2ZrF_6 was excluded because of its high Li-ion migration barrier.

As illustrated in Fig. 5b, lithium fluorides generally present good compatibility toward LFP, FP, and LGPS. Specifically,

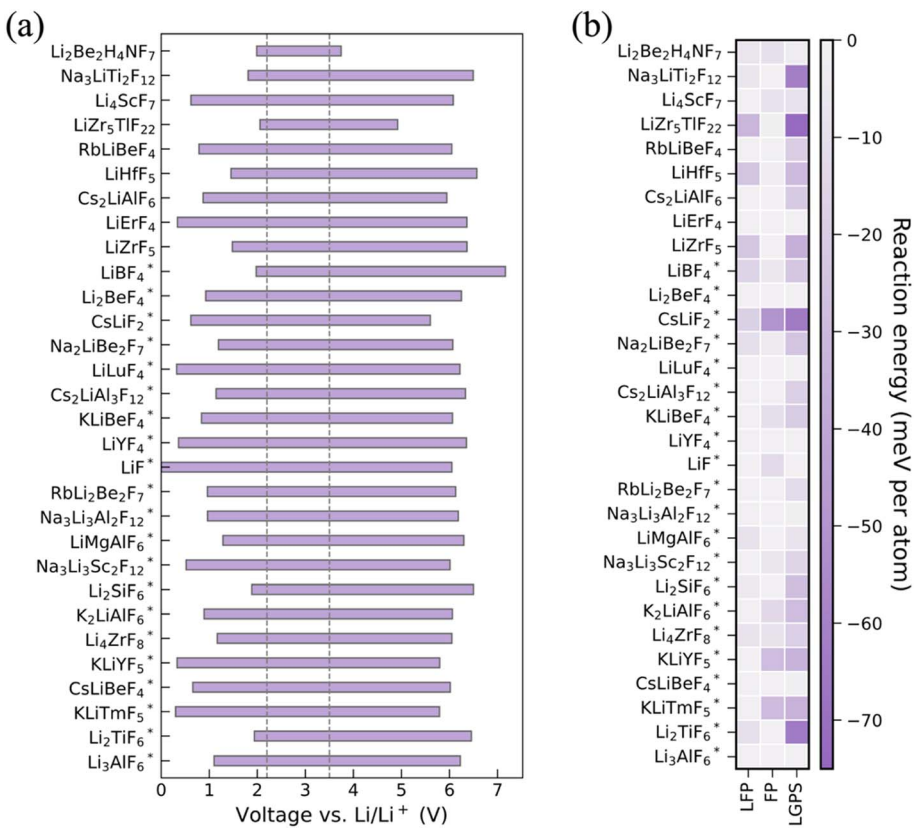

Fig. 5 (a) Electrochemical stability windows of various fluorides. (b) Chemical reactivity of fluorides with LFP, FP, and LGPS.

Li_3AlF_6, $LiYF_4$, $LiLuF_4$, Li_2BeF_4, and $LiErF_4$ exhibit no chemical reactivity with the three phases, indicating their very promising performance as coatings. Despite usage in batteries with liquid electrolytes, Li_2TiF_6 demonstrates a non-trivial reactivity with LGPS with a ΔE_{rxt} of −64 meV per atom, limiting its applications considered in this work. Nevertheless, fluorides remain a promising class of materials that are suitable for use in LFP-based ASSBs with sulfide electrolytes.

3.3.3 Phosphates. Apart from lithium ternary metal oxides, lithium phosphates are another extensively applied category of coating materials. Li_3PO_4, $LiTi_2(PO_4)_3$, and $LiMgPO_4$ have been employed as cathode coatings in batteries with liquid electrolytes.[51–53] Specifically, a Li_3PO_4-coated LFP cathode demonstrates improved rate and cycling performance. As shown in Fig. 6, these three compounds are also involved in our screening results. Based on a computational screening, Xiao *et al.* proposed two other new lithium phosphates as potential coatings for high-voltage cathodes, including LiH_2PO_4 and $LiPO_3$.[11] However, they are excluded from our screening workflow because they exceed the selected electrochemical reduction limits, with LiH_2PO_4 and $LiPO_3$ exhibiting a V_{red} of 2.3 and 2.5 V, respectively.

As depicted in Fig. 6a, compared to NP oxides, all nine phosphates demonstrate a larger V_{ox} of over 4 V. The enhanced electrochemical oxidation resistance of phosphates can be attributed to the inductive effect, which is often exploited to increase the operating voltages of electrodes. Due to the similarity of anionic units, these phosphates all present excellent interfacial compatibility with LFP and FP, with a $|\Delta E_{rxt}|$ smaller

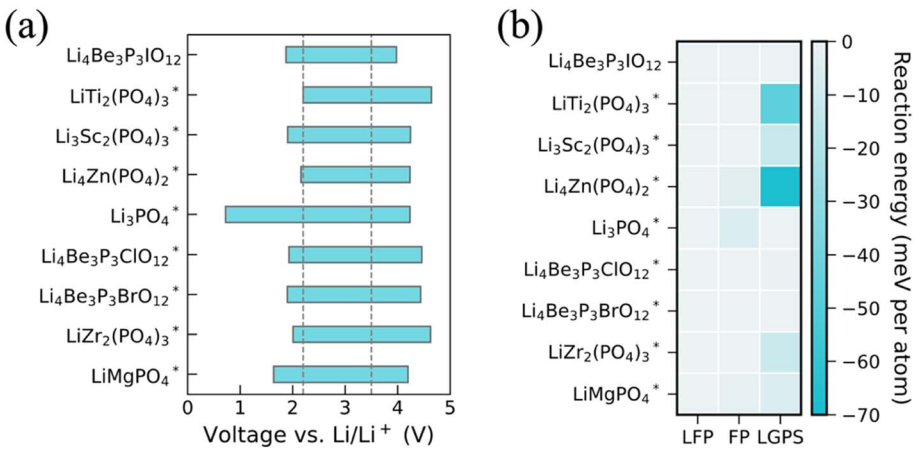

Fig. 6 (a) Electrochemical stability windows of various phosphates. (b) Chemical reactivity of phosphates with LFP, FP, and LGPS.

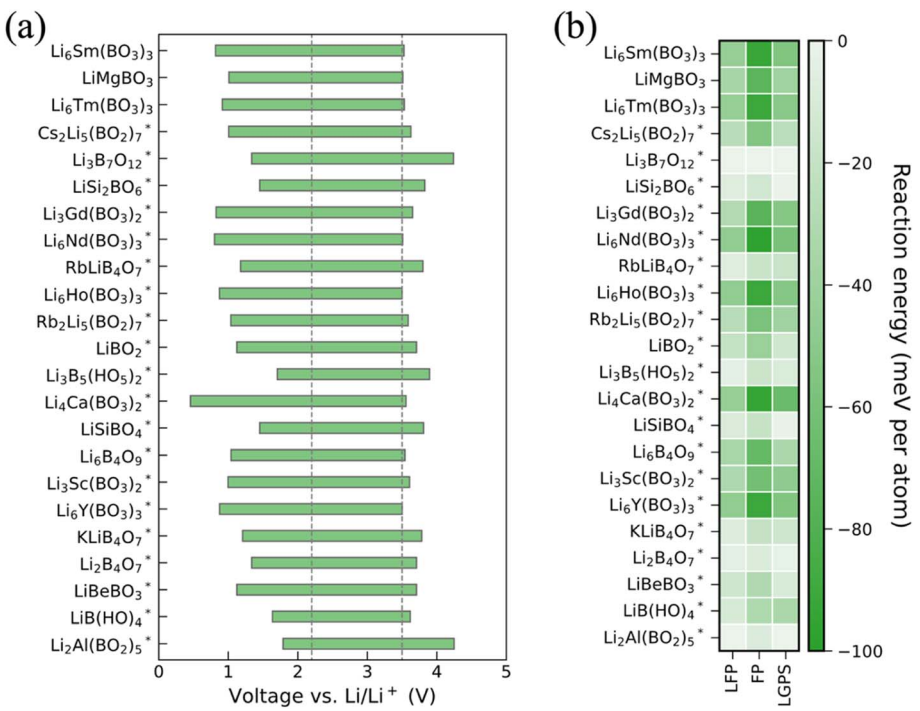

Fig. 7 (a) Electrochemical stability windows of various borates. (b) Chemical reactivity of borates with LFP, FP, and LGPS.

than 10 meV per atom. In terms of the compatibility toward sulfide electrolytes, these compounds generally show negligible reactivity with LGPS, except for $LiTi_2(PO_4)_3$ ($\Delta E_{rxt} = -47$ meV per atom) and $Li_4Zn(PO_4)_2$ ($\Delta E_{rxt} = -68$ meV per atom). Hence, it is evident that lithium phosphates may exhibit appealing performance for coating LFP active materials in ASSBs with sulfide electrolytes.

3.3.4 Borates. Lithium borates are a fairly unexplored category of cathode coatings. Recently, Li_3BO_3 and $Li_2B_4O_7$ have been proposed as appealing buffer layers for high-voltage cathodes.[54,55] From Fig. 7, $Li_2B_4O_7$ is involved in our screening results. Li_3BO_3 is screened out because of its strong reactivity with FP, with an ΔE_{rxt} of -112 meV per atom. As depicted in Fig. 7b, $Li_3B_7O_{12}$, $Li_2B_4O_7$, and $Li_2Al(BO_2)_5$ demonstrate perfect interfacial compatibility toward LFP, FP, and LGPS, with a $|\Delta E_{rxt}|$ lower than 10 meV per atom. Specifically, $Li_3B_7O_{12}$ exhibits no reactivity with the three phases, implying its potential good performance as a coating material. However, as depicted in Fig. 7b, the majority of the lithium borates still exhibit favorable reactivity with LFP, FP, and LGPS.

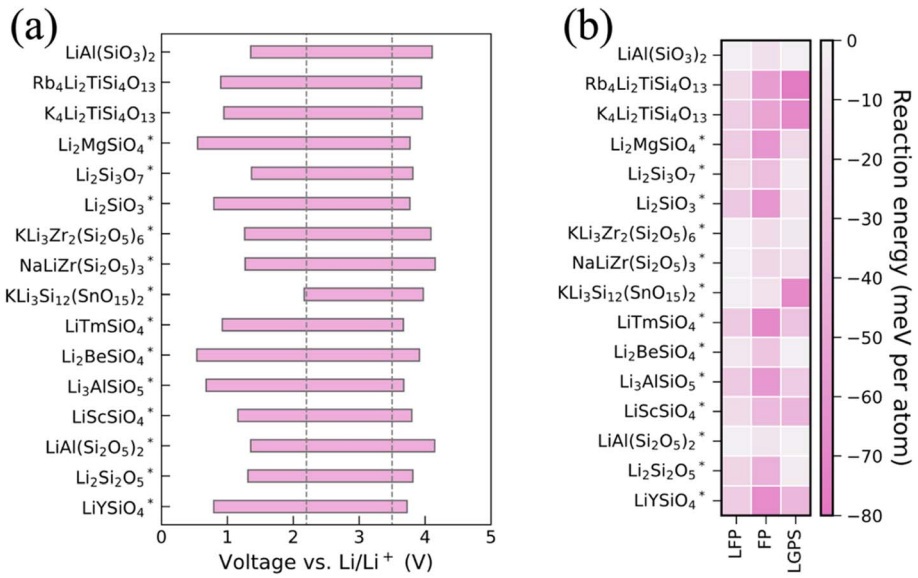

Fig. 8 (a) Electrochemical stability windows of various silicates. (b) Chemical reactivity of silicates with LFP, FP, and LGPS.

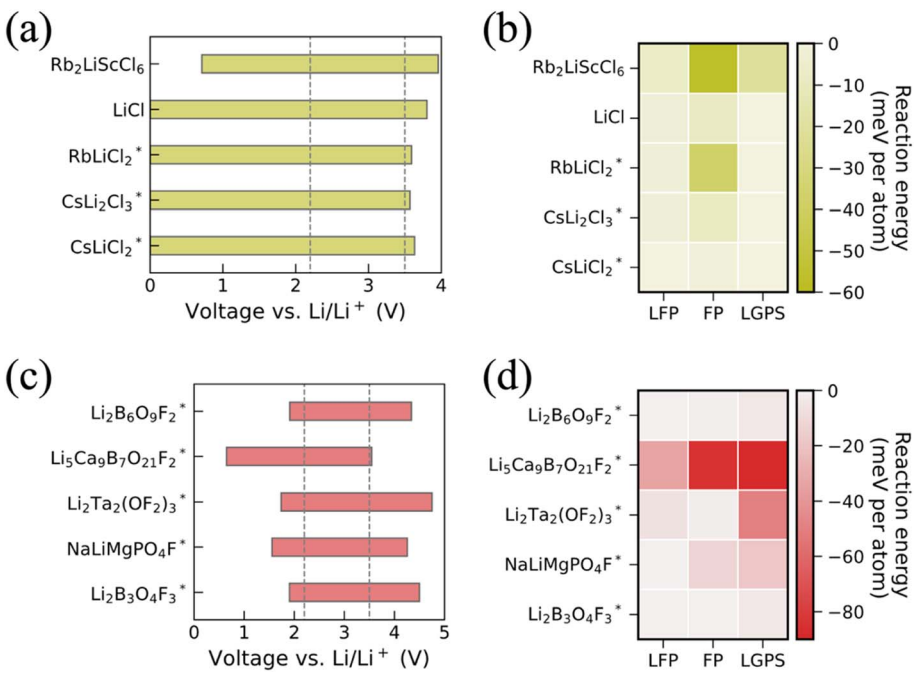

Fig. 9 (a) Electrochemical stability windows of various chlorides. (b) Chemical reactivity of chlorides with LFP, FP, and LGPS. (c) Electrochemical stability windows of oxyfluorides. (d) Chemical reactivity of various oxyfluorides with LFP, FP, and LGPS.

3.3.5 Silicates. To date, only a limited number of lithium silicates have been employed as cathode coatings, including Li_2SiO_3, Li_4SiO_4, and $Li_2Si_2O_5$.[56–58] From Fig. 8, Li_2SiO_3 and $Li_2Si_2O_5$ are included in our preliminary screening results. For Li_4SiO_4, we predicted a strong reactivity between it and FP, with an ΔE_{rxt} of −115 meV per atom. As in the case of lithium borates, from Fig. 8b, most of the screened lithium silicates still showcase favorable reactivity with LFP, FP, or LGPS. Even for Li_2SiO_3 and $Li_2Si_2O_5$, both exhibit non-trivial reactivity with FP, with the decomposition products of Fe_2O_3, Li_3PO_4, and SiO_2.

3.3.5 Others. Finally, our screening workflow returned five lithium chlorides and five lithium oxyfluorides. As shown in Fig. 9a, chlorides demonstrate very promising electrochemical reduction resistance, with the V_{red} even reaching 0 V. On the other hand, compared to NP oxides, oxyfluorides exhibit improved oxidation limits (Fig. 9c), which can be attributed to the inclusion of fluorine. In terms of the interfacial compatibility, these screened materials generally demonstrate inert reactivity with LFP, FP, and LGPS. Hence, lithium chlorides and lithium oxyfluorides are appealing classes of coating materials for LFP-based ASSBs with sulfide electrolytes.

3.4 Summarization of promising coating materials

Building upon the initial screening results, we compiled a list of coating materials that exhibit exceptional compatibility with LFP, FP, and LGPS simultaneously, as illustrated in Table 1. To allow for some potential kinetic stabilization, we set the

Table 1 Promising coating candidates for usage in LFP-based ASSBs with sulfide electrolytes. For those compounds whose NEB calculations did not converge (marked with *), their BV barriers were represented instead

	Identity		Reaction energy (meV per atom)			Electrochemical window (V)		
Formula	Atomly ID	ICSD	LFP	FP	LGPS	Reduction	Oxidation	Migration barrier (meV)
Li_3AlF_6	0000093303	85 171	0	0	0	1.10	6.22	462
$CsLiBeF_4$	0000020963	9434	0	0	−1	0.66	6.02	1034
Li_4ZrF_8	0000032607	80 398	−7	−8	−18	1.17	6.05	386
$Na_3Li_3Sc_2F_{12}$	0000101912	27 007	0	−6	−15	0.52	6.01	371
$LiMgAlF_6$	0000006756	5007	−8	0	−7	1.29	6.30	610
$Na_3Li_3Al_2F_{12}$	0000105344	9923	0	0	−1	0.96	6.18	295
$RbLi_2Be_2F_7$	0000010397	72	0	0	−11	0.96	6.13	467
LiF	0000057894	41 409	0	−12	0	0	6.05	631
$LiYF_4$	0000002504	96 727	0	0	0	0.36	6.35	502
$KLiBeF_4$	0000020198	2939	0	−10	−20	0.84	6.06	1350
$Cs_2LiAl_3F_{12}$	0000099318	15 785	0	0	−18	1.14	6.33	354*
$LiLuF_4$	0000036754	152 948	0	0	0	0.32	6.22	473
Li_2BeF_4	0000004787	14 360	0	0	0	0.93	6.25	365
$LiErF_4$	3001234939	—	0	0	0	0.34	6.36	589*
$RbLiBeF_4$	3001345161	—	0	0	−19	0.79	6.05	564*
Li_4ScF_7	3001070431	—	0	−9	−9	0.62	6.08	85
$LiMgPO_4$	0000083694	201 138	0	−2	−6	1.64	4.20	285
$LiZr_2(PO_4)_3$	0000018210	91 112	0	0	−11	2.01	4.62	1078
$Li_4Be_3P_3BrO_{12}$	0000114496	80 472	0	0	0	1.90	4.44	762
$Li_4Be_3P_3ClO_{12}$	0000028543	74 525	0	0	−1	1.93	4.46	691
Li_3PO_4	0000061102	10 257	0	−6	0	0.72	4.23	428
$Li_3Sc(PO_4)_3$	0000110893	62 301	0	0	−12	1.91	4.25	371
$Li_4Be_3P_3IO_{12}$	0000041332	—	0	0	0	1.87	3.98	913
$Li_2Al(BO_2)_5$	0000125099	279 578	0	−8	0	1.79	4.25	354
$Li_2B_4O_7$	0000030688	34 670	−5	−8	−3	1.34	3.71	69
$KLiB_4O_7$	0000088006	93 601	−8	−20	−16	1.21	3.78	383
$LiSiBO_4$	0000088234	67 536	−9	−20	−1	1.45	3.81	759
$Li_3B_5(HO_5)_2$	0000117025	20 155	−3	−18	−9	1.70	3.90	659
$RbLiB_4O_7$	0000005274	93 602	−7	−18	−18	1.18	3.80	143
$LiSi_2BO_6$	0000070152	90 849	−7	−14	0	1.45	3.83	633
$Li_3B_7O_{12}$	0000026116	68 475	0	0	0	1.34	4.24	645
$LiAl(Si_2O_5)_2$	0000063234	31 283	0	−7	0	1.35	4.15	1016
$NaLiZr(Si_2O_5)_3$	0000078334	100 631	0	−16	−12	1.27	4.15	1415
$KLi_3Zr_2(Si_2O_5)_6$	0000013946	89 899	0	−14	−5	1.26	4.09	1273
$LiAl(SiO_3)_2$	0000058662	—	0	−10	0	1.35	4.11	520
$CsLiCl_2$	3001483162	423 634	0	−1	0	0	3.63	466
$CsLi_2Cl_3$	0000045002	423 635	−2	−9	0	0	3.57	617
LiCl	0000122077	—	−2	−9	0	0	3.80	399
$Li_2B_3O_4F_3$	0000028336	423 661	0	0	−5	1.90	4.50	541
$NaLiMgPO_4F$	0000087290	426 199	0	−13	−18	1.56	4.26	1150
$Li_2B_6O_9F_2$	0000054059	423 435	0	−1	−4	1.91	4.34	274

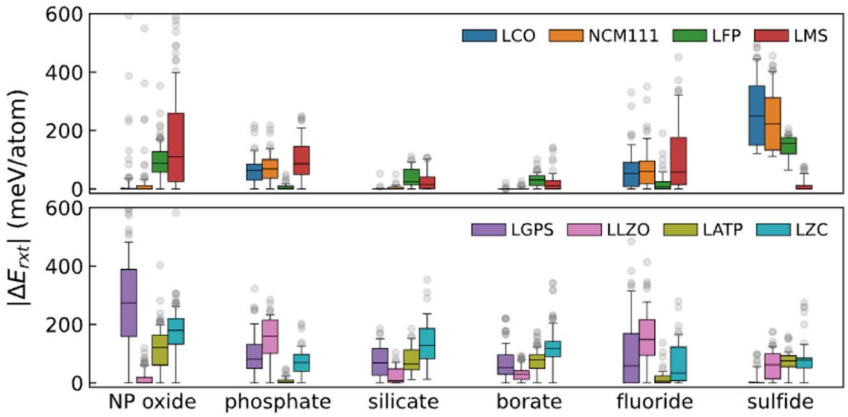

Fig. 10 Chemical reactivity of different compositions with various types of cathodes and electrolytes. The types of compositions include NP oxides, phosphates, silicates, borates, fluorides, and sulfides. The types of cathodes include LCO, NCM111, LFP, and $LiMnS_2$ (LMS). The types of electrolytes include LGPS, LLZO, $Li_{1.3}Al_{0.3}Ti_{1.7}(PO_4)_3$ (LATP), and Li_2ZrCl_6 (LZC). Each box represents the quartiles of the dataset (gray dots), and the whisker extends to show the rest of the distribution.

threshold for negligible interfacial reactivity to be −20 meV per atom. To accurately evaluate the ionic conductivities of these coating candidates, we conducted NEB calculations for the single Li-ion vacancy migration barrier (detailed migration profiles are depicted in Fig. S1–S41, ESI†). Experimentally, a coating layer can have a well-controlled thickness of ∼1–20 nm.[9] This suggests that materials with moderate ionic conductivities within the range of 10^{-7}–10^{-9} S cm^{-1} will be sufficiently effective for coating applications. As depicted in Table 1, the majority of the coating candidates demonstrate moderate-to-low migration barriers, typically not exceeding 0.7 eV, implying their favorable kinetic performance in the context of cathode coatings.

4. Discussion

It is a complex challenge to determine the interfacial compatibility between materials with different chemical compositions. In this work, by categorizing potential LFP coating compounds into seven chemical groups, it has been demonstrated that anionic chemistry plays a significant role in determining the reactivity between two materials in contact. For instance, we have identified a general trend in which lithium ternary oxides typically display significantly more favorable reactivity toward LFP compared to LCO or LNO.

While this study primarily focused on addressing contact issues between LFP and sulfide electrolytes, a comprehensive evaluation of interfacial compatibility across various chemistries is essential to provide further guidance for coating selection. As illustrated in Fig. 10, we performed a statistical analysis of the reactivity between different pairs of chemical compositions. Several rules of thumb can be derived: (1) materials with the same anionic chemistry generally showcase exceptional chemical compatibility, (2) NP oxides normally demonstrate favorable reactivity toward phosphorus-containing compounds, (3) compatibility between fluorides and phosphates is outstanding, and (4) silicates and borates generally exhibit negligible reactivity with all types of cathode materials with varying anionic chemistries, spanning from layered oxides and polyanionic oxides, to layered sulfides.

From the lower panel in Fig. 10, sulfide electrolytes, such as LGPS, generally demonstrate poor compatibility with various chemical compositions, except for sulfides (sulfides cannot be used as coatings because of their inherently narrow electrochemical windows), which poses a significant challenge for coating selection in ASSBs with sulfide electrolytes. However, despite a relatively high average $|\Delta E_{rxt}|$ of 108 meV per atom between LGPS and fluorides, twenty-five percent of fluorides showcase no reactivity toward LGPS. This suggests that fluorides are a superior choice of coating materials for ASSBs utilizing sulfide electrolytes, aligning with the discussion in Section 3.3.

It is widely recognized that LFP is a poor electronic conductor, which imposes limitations on the rate performance of LFP-based batteries. Experimental evidence has indicated that the deposition of carbon on LFP particles is a crucial process for enhancing the power capability of the cathode composite.[2] This raises a significant paradox in the context of the coating strategy discussed in this work, as carbon coatings cannot protect sulfide-based SSEs from electrochemical oxidation. To mitigate this concern, an effective strategy may be coating LFP particles with a hybrid coating composite consisting of both carbon and an electronic insulator.[59,60]

5. Conclusions

LFP batteries have emerged as a viable alternative to commercial lithium-ion battery (LiB) technologies that use layered Co-based cathodes. As LiBs advance toward the ASSB phase, a systematic screening was conducted to identify the most promising coating compounds that can reconcile the (electro) chemical reactions between LFP and sulfide-based SSEs. This study identified several potential coating materials from a pool of 54 005 lithium-containing compounds. The screening

process was comprehensive, taking into account factors such as thermodynamic stability, electronic conductance, electrochemical stability window, chemical reactivity, and ionic conductance. The results indicated that fluorine-, chlorine-, and phosphorus-containing compounds generally outperformed NP oxides when utilized as interfacial compounds between LFP and SSEs. Following further scrutiny of their reactions with LGPS, a select few compounds emerged as the best candidates and are listed in Table 1. This research illustrates the effective application of a protocol for the virtual design, screening, and evaluation of electrochemically inert materials from a wide-ranging pool of prospective compounds. Though this methodology builds on existing literature, prior studies mainly concentrated on layered cathodes. This paper effectively broadens the scope, offering valuable insights for engineering electrolyte–electrode interfaces within LFP-based ASSBs.

Author contributions

Conceptualization: M. L. and T. L. Methodology: M. L. and T. L. Investigation: T. L. Funding acquisition: M. L. and S. M. Software: T. L. Supervision: M. L. and S. M. Writing – original draft: T. L. and M. L. Writing – review and editing: M. L. and S. M.

Conflicts of interest

The authors declare no conflict of interest.

Acknowledgements

This research was supported by the National Key R&D Program of China (2021YFA0718700), the Chinese Academy of Sciences (Grant No. CAS-WX2023SF-0101, ZDBS-LY-SLH007, XDB33020000, XDB33030100, and YSBR-047), and the National Natural Science Foundation of China (Grant No. 12025407 and 11934003). The computational resource is provided by the Platform for Data-Driven Computational Materials Discovery of the Songshan Lake laboratory.

References

1 A. K. Padhi, K. S. Nanjundaswamy and J. B. Goodenough, Phospho-olivines as Positive-Electrode Materials for Rechargeable Lithium Batteries, *J. Electrochem. Soc.*, 1997, **144**(4), 1188–1194, DOI: **10.1149/1.1837571**.

2 L.-X. Yuan, Z.-H. Wang, W.-X. Zhang, X.-L. Hu, J.-T. Chen, Y.-H. Huang and J. B. Goodenough, Development and Challenges of $LiFePO_4$ Cathode Material for Lithium-Ion Batteries, *Energy Environ. Sci.*, 2011, **4**(2), 269–284, DOI: **10.1039/C0EE00029A**.

3 N. Kamaya, K. Homma, Y. Yamakawa, M. Hirayama, R. Kanno, M. Yonemura, T. Kamiyama, Y. Kato, S. Hama, K. Kawamoto and A. Mitsui, A Lithium Superionic Conductor, *Nat. Mater.*, 2011, **10**(9), 682–686, DOI: **10.1038/nmat3066**.

4 Z. Zhang, Y. Shao, B. Lotsch, Y.-S. Hu, H. Li, J. Janek, L. F. Nazar, C.-W. Nan, J. Maier, M. Armand and L. Chen, New Horizons for Inorganic Solid State Ion Conductors, *Energy Environ. Sci.*, 2018, **11**(8), 1945–1976, DOI: **10.1039/C8EE01053F**.

5 V. Thangadurai, S. Narayanan and D. Pinzaru, Garnet-Type Solid-State Fast Li Ion Conductors for Li Batteries: Critical Review, *Chem. Soc. Rev.*, 2014, **43**(13), 4714, DOI: **10.1039/c4cs00020j**.

6 Y. Li, S. Song, H. Kim, K. Nomoto, H. Kim, X. Sun, S. Hori, K. Suzuki, N. Matsui, M. Hirayama, T. Mizoguchi, T. Saito, T. Kamiyama and R. Kanno, A Lithium Superionic Conductor for Millimeter-Thick Battery Electrode, *Science*, 2023, **381**(6653), 50–53, DOI: **10.1126/science.add7138**.

7 X. Yan, Z. Li, Z. Wen and W. Han, $Li/Li_7La_3Zr_2O_{12}/LiFePO_4$ All-Solid-State Battery with Ultrathin Nanoscale Solid Electrolyte, *J. Phys. Chem. C*, 2017, **121**(3), 1431–1435, DOI: **10.1021/acs.jpcc.6b10268**.

8 Y. Seino, T. Ota, K. Takada, A. Hayashi and M. Tatsumisago, A Sulphide Lithium Super Ion Conductor Is Superior to Liquid Ion Conductors for Use in Rechargeable Batteries, *Energy Environ. Sci.*, 2014, **7**(2), 627–631, DOI: **10.1039/C3EE41655K**.

9 Y. Xiao, Y. Wang, S.-H. Bo, J. C. Kim, L. J. Miara and G. Ceder, Understanding Interface Stability in Solid-State Batteries, *Nat. Rev. Mater.*, 2020, **5**(2), 105–126, DOI: **10.1038/s41578-019-0157-5**.

10 Y. Zhu, X. He and Y. Mo, First Principles Study on Electrochemical and Chemical Stability of Solid Electrolyte–Electrode Interfaces in All-Solid-State Li-Ion Batteries, *J. Mater. Chem. A*, 2016, **4**(9), 3253–3266, DOI: **10.1039/C5TA08574H**.

11 Y. Xiao, L. J. Miara, Y. Wang and G. Ceder, Computational Screening of Cathode Coatings for Solid-State Batteries, *Joule*, 2019, **3**(5), 1252–1275, DOI: **10.1016/j.joule.2019.02.006**.

12 *Atomly*, **https://atomly.net**, accessed 2023-10-13.

13 M. Liu and S. M. Atomly, Net Materials Database and Its Application in Inorganic Chemistry, *Sci. Sin.: Chim.*, 2023, **53**(1), 19–25.

14 G. Kresse and D. Joubert, From Ultrasoft Pseudopotentials to the Projector Augmented-Wave Method, *Phys. Rev. B*, 1999, **59**(3), 1758–1775, DOI: **10.1103/PhysRevB.59.1758**.

15 G. Kresse and J. Furthmüller, Efficiency of Ab-Initio Total Energy Calculations for Metals and Semiconductors Using a Plane-Wave Basis Set, *Comput. Mater. Sci.*, 1996, **6**(1), 15–50, DOI: **10.1016/0927-0256(96)00008-0**.

16 J. P. Perdew, K. Burke and M. Ernzerhof, Generalized Gradient Approximation Made Simple, *Phys. Rev. Lett.*, 1996, **77**(18), 3865–3868, DOI: **10.1103/PhysRevLett.77.3865**.

17 T. Lu, Y. Wang, G. Cai, H. Jia, X. Liu, C. Zhang, S. Meng and M. Liu, Synthesizability of Transition-Metal Dichalcogenides: A Systematic First-Principles Evaluation, *Materials Futures*, 2023, **2**(1), 015001, DOI: **10.1088/2752-5724/acbe10**.

18 Y. Liang, M. Chen, Y. Wang, H. Jia, T. Lu, F. Xie, G. Cai, Z. Wang, S. Meng and M. Liu, A Universal Model for Accurately Predicting the Formation Energy of Inorganic

Compounds, *Sci. China Mater.*, 2023, **66**(1), 343–351, DOI: 10.1007/s40843-022-2134-3.

19 T. Lu, S. Meng and M. Liu, Weberite Na2MM'F7 (M,M'=Redox-Active Metal) as Promising Fluoride-Based Sodium-Ion Battery Cathodes, *arXiv*, 2023, preprint, arXiv:2310.04222, DOI: 10.48550/arXiv.2310.04222.

20 Y. Jiang, Z. Yu, Y. Wang, T. Lu, S. Meng, K. Jiang and M. Liu, Screening Promising CsV_3Sb_5-Like Kagome Materials from Systematic First-Principles Evaluation, *Chin. Phys. Lett.*, 2022, **39**(4), 047402, DOI: 10.1088/0256-307X/39/4/047402.

21 F. Xie, T. Lu, Z. Yu, Y. Wang, Z. Wang, S. Meng and M. Liu, Lu–H–N Phase Diagram from First-Principles Calculations, *Chin. Phys. Lett.*, 2023, **40**(5), 057401, DOI: 10.1088/0256-307X/40/5/057401.

22 S. P. Ong, W. D. Richards, A. Jain, G. Hautier, M. Kocher, S. Cholia, D. Gunter, V. L. Chevrier, K. A. Persson and G. Ceder, Python Materials Genomics (Pymatgen): A Robust, Open-Source Python Library for Materials Analysis, *Comput. Mater. Sci.*, 2013, **68**, 314–319, DOI: 10.1016/j.commatsci.2012.10.028.

23 W. D. Richards, L. J. Miara, Y. Wang, J. C. Kim and G. Ceder, Interface Stability in Solid-State Batteries, *Chem. Mater.*, 2016, **28**(1), 266–273, DOI: 10.1021/acs.chemmater.5b04082.

24 L. L. Wong, K. C. Phuah, R. Dai, H. Chen, W. S. Chew and S. Adams, Bond Valence Pathway Analyzer—An Automatic Rapid Screening Tool for Fast Ion Conductors within softBV, *Chem. Mater.*, 2021, **33**(2), 625–641, DOI: 10.1021/acs.chemmater.0c03893.

25 G. Henkelman, B. P. Uberuaga and H. Jónsson, A Climbing Image Nudged Elastic Band Method for Finding Saddle Points and Minimum Energy Paths, *J. Chem. Phys.*, 2000, **113**(22), 9901–9904, DOI: 10.1063/1.1329672.

26 G. Henkelman and H. Jónsson, Improved Tangent Estimate in the Nudged Elastic Band Method for Finding Minimum Energy Paths and Saddle Points, *J. Chem. Phys.*, 2000, **113**(22), 9978–9985, DOI: 10.1063/1.1323224.

27 G. Oh, M. Hirayama, O. Kwon, K. Suzuki and R. Kanno, Bulk-Type All Solid-State Batteries with 5 V Class $LiNi_{0.5}Mn_{1.5}O_4$ Cathode and $Li_{10}GeP_2S_{12}$ Solid Electrolyte, *Chem. Mater.*, 2016, **28**(8), 2634–2640, DOI: 10.1021/acs.chemmater.5b04940.

28 X. Li, J. Liu, M. N. Banis, A. Lushington, R. Li, M. Cai and X. Sun, Atomic Layer Deposition of Solid-State Electrolyte Coated Cathode Materials with Superior High-Voltage Cycling Behavior for Lithium Ion Battery Application, *Energy Environ. Sci.*, 2014, **7**(2), 768–778, DOI: 10.1039/C3EE42704H.

29 J. Chong, J. Zhang, H. Xie, X. Song, G. Liu, V. Battaglia, S. Xun and R. Wang, High Performance $LiNi_{0.5}Mn_{1.5}O_4$ Cathode Material with a Bi-Functional Coating for Lithium Ion Batteries, *RSC Adv.*, 2016, **6**(23), 19245–19251, DOI: 10.1039/C6RA00119J.

30 M. Aykol, S. Kim, V. I. Hegde, D. Snydacker, Z. Lu, S. Hao, S. Kirklin, D. Morgan and C. Wolverton, High-Throughput Computational Design of Cathode Coatings for Li-Ion Batteries, *Nat. Commun.*, 2016, **7**(1), 13779, DOI: 10.1038/ncomms13779.

31 T. Kaib, S. Haddadpour, M. Kapitein, P. Bron, C. Schröder, H. Eckert, B. Roling and S. Dehnen, New Lithium Chalcogenidotetrelates, LiChT: Synthesis and Characterization of the Li^+-Conducting Tetralithium *Ortho*-Sulfidostannate Li_4SnS_4, *Chem. Mater.*, 2012, **24**(11), 2211–2219, DOI: 10.1021/cm3011315.

32 E. Rangasamy, Z. Liu, M. Gobet, K. Pilar, G. Sahu, W. Zhou, H. Wu, S. Greenbaum and C. Liang, An Iodide-Based $Li_7P_2S_8I$ Superionic Conductor, *J. Am. Chem. Soc.*, 2015, **137**(4), 1384–1387, DOI: 10.1021/ja508723m.

33 J. Auvergniot, A. Cassel, J.-B. Ledeuil, V. Viallet, V. Seznec and R. Dedryvère, Interface Stability of Argyrodite Li_6PS_5Cl toward $LiCoO_2$, $LiNi_{1/3}Co_{1/3}Mn_{1/3}O_2$, and $LiMn_2O_4$ in Bulk All-Solid-State Batteries, *Chem. Mater.*, 2017, **29**(9), 3883–3890, DOI: 10.1021/acs.chemmater.6b04990.

34 P. Adeli, J. D. Bazak, K. H. Park, I. Kochetkov, A. Huq, G. R. Goward and L. F. Nazar, Boosting Solid-State Diffusivity and Conductivity in Lithium Superionic Argyrodites by Halide Substitution, *Angew. Chem., Int. Ed.*, 2019, **58**(26), 8681–8686, DOI: 10.1002/anie.201814222.

35 Z. Liu, W. Fu, E. A. Payzant, X. Yu, Z. Wu, N. J. Dudney, J. Kiggans, K. Hong, A. J. Rondinone and C. Liang, Anomalous High Ionic Conductivity of Nanoporous β-Li_3PS_4, *J. Am. Chem. Soc.*, 2013, **135**(3), 975–978, DOI: 10.1021/ja3110895.

36 R. Kanno and M. Murayama, Lithium Ionic Conductor Thio-LISICON: The Li_2S-GeS_2-P_2S_5 System, *J. Electrochem. Soc.*, 2001, **148**(7), A742, DOI: 10.1149/1.1379028.

37 A. Cronk, Y.-T. Chen, G. Deysher, S.-Y. Ham, H. Yang, P. Ridley, B. Sayahpour, L. H. B. Nguyen, J. A. S. Oh, J. Jang, D. H. S. Tan and Y. S. Meng, Overcoming the Interfacial Challenges of $LiFePO_4$ in Inorganic All-Solid-State Batteries, *ACS Energy Lett.*, 2023, **8**(1), 827–835, DOI: 10.1021/acsenergylett.2c02138.

38 J.-S. Kim, C. S. Johnson, J. T. Vaughey, S. A. Hackney, K. A. Walz, W. A. Zeltner, M. A. Anderson and M. M. Thackeray, The Electrochemical Stability of Spinel Electrodes Coated with ZrO_2, Al_2O_3, and SiO_2 from Colloidal Suspensions, *J. Electrochem. Soc.*, 2004, **151**(10), A1755, DOI: 10.1149/1.1793713.

39 Y.-K. Sun, J.-M. Han, S.-T. Myung, S.-W. Lee and K. Amine, Significant Improvement of High Voltage Cycling Behavior AlF_3-Coated $LiCoO_2$ Cathode, *Electrochem. Commun.*, 2006, **8**(5), 821–826, DOI: 10.1016/j.elecom.2006.03.040.

40 Y. Zhu, X. He and Y. Mo, Origin of Outstanding Stability in the Lithium Solid Electrolyte Materials: Insights from Thermodynamic Analyses Based on First-Principles Calculations, *ACS Appl. Mater. Interfaces*, 2015, **7**(42), 23685–23693, DOI: 10.1021/acsami.5b07517.

41 K. Okada, N. Machida, M. Naito, T. Shigematsu, S. Ito, S. Fujiki, M. Nakano and Y. Aihara, Preparation and Electrochemical Properties of $LiAlO_2$-Coated $Li(Ni_{1/3}Mn_{1/3}Co_{1/3})O_2$ for All-Solid-State Batteries, *Solid State Ionics*, 2014, **255**, 120–127, DOI: 10.1016/j.ssi.2013.12.019.

42 K. Takada, N. Ohta, L. Zhang, K. Fukuda, I. Sakaguchi, R. Ma, M. Osada and T. Sasaki, Interfacial Modification for

High-Power Solid-State Lithium Batteries, *Solid State Ionics*, 2008, **179**(27), 1333–1337, DOI: 10.1016/j.ssi.2008.02.017.

43 S. Ito, S. Fujiki, T. Yamada, Y. Aihara, Y. Park, T. Y. Kim, S.-W. Baek, J.-M. Lee, S. Doo and N. Machida, A Rocking Chair Type All-Solid-State Lithium Ion Battery Adopting Li_2O–ZrO_2 Coated $LiNi_{0.8}Co_{0.15}Al_{0.05}O_2$ and a Sulfide Based Electrolyte, *J. Power Sources*, 2014, **248**, 943–950, DOI: 10.1016/j.jpowsour.2013.10.005.

44 N. Ohta, K. Takada, L. Zhang, R. Ma, M. Osada and T. Sasaki, Enhancement of the High-Rate Capability of Solid-State Lithium Batteries by Nanoscale Interfacial Modification, *Adv. Mater.*, 2006, **18**(17), 2226–2229, DOI: 10.1002/adma.200502604.

45 K. Takada, N. Ohta, L. Zhang, X. Xu, B. T. Hang, T. Ohnishi, M. Osada and T. Sasaki, Interfacial Phenomena in Solid-State Lithium Battery with Sulfide Solid Electrolyte, *Solid State Ionics*, 2012, **225**, 594–597, DOI: 10.1016/j.ssi.2012.01.009.

46 F. Walther, F. Strauss, X. Wu, B. Mogwitz, J. Hertle, J. Sann, M. Rohnke, T. Brezesinski and J. Janek, The Working Principle of a Li_2CO_3/$LiNbO_3$ Coating on NCM for Thiophosphate-Based All-Solid-State Batteries, *Chem. Mater.*, 2021, **33**(6), 2110–2125, DOI: 10.1021/acs.chemmater.0c04660.

47 K. Okada, N. Machida, M. Naito, T. Shigematsu, S. Ito, S. Fujiki, M. Nakano and Y. Aihara, Preparation and Electrochemical Properties of $LiAlO_2$-Coated $Li(Ni_{1/3}Mn_{1/3}Co_{1/3})O_2$ for All-Solid-State Batteries, *Solid State Ionics*, 2014, **255**, 120–127, DOI: 10.1016/j.ssi.2013.12.019.

48 W. Choi, A. Benayard, J.-H. Park, J. Park, S.-G. Doo and J. Mun, Versatile Coating of Lithium Conductive Li_2TiF_6 on Over-Lithiated Layered Oxide in Lithium-Ion Batteries, *Electrochim. Acta*, 2014, **117**, 492–497, DOI: 10.1016/j.electacta.2013.11.184.

49 J. Xie, A. D. Sendek, E. D. Cubuk, X. Zhang, Z. Lu, Y. Gong, T. Wu, F. Shi, W. Liu, E. J. Reed and Y. Cui, Atomic Layer Deposition of Stable $LiAlF_4$ Lithium Ion Conductive Interfacial Layer for Stable Cathode Cycling, *ACS Nano*, 2017, **11**(7), 7019–7027, DOI: 10.1021/acsnano.7b02561.

50 J. Fan, T. Dong, D. Fang, X. Li, X. Mo, K. Wen, S. Chen and S. Zhang, A Lithium Salt Additive Li_2ZrF_6 for Enhancing the Electrochemical Performance of High-Voltage $LiNi_{0.5}Mn_{1.5}O_4$ Cathode, *Ionics*, 2018, **24**(10), 2965–2972, DOI: 10.1007/s11581-018-2512-8.

51 L.-L. Zhang, J.-Q. Wang, X.-L. Yang, G. Liang, T. Li, P.-L. Yu and D. Ma, Enhanced Electrochemical Performance of Fast Ionic Conductor $LiTi_2(PO_4)_3$-Coated $LiNi_{1/3}Co_{1/3}Mn_{1/3}O_2$ Cathode Material, *ACS Appl. Mater. Interfaces*, 2018, **10**(14), 11663–11670, DOI: 10.1021/acsami.7b19692.

52 H. Morimoto, H. Awano, J. Terashima, S. Nakanishi, Y. Hirama, K. Ishikawa and S. Tobishima, Charge–Discharge Properties of $LiCoO_2$ Electrodes Modified by Olivine-Type Compounds of $LiMgPO_4$ for Lithium Secondary Batteries, *J. Power Sources*, 2012, **211**, 66–70, DOI: 10.1016/j.jpowsour.2012.03.044.

53 K. Takahashi, K. Hattori, T. Yamazaki, K. Takada, M. Matsuo, S. Orimo, H. Maekawa and H. Takamura, All-Solid-State Lithium Battery with $LiBH_4$ Solid Electrolyte, *J. Power Sources*, 2013, **226**, 61–64, DOI: 10.1016/j.jpowsour.2012.10.079.

54 Y. Charles-Blin, K. Nemoto, N. Zettsu and K. Teshima, Effects of a Solid Electrolyte Coating on the Discharge Kinetics of a $LiCoO_2$ Electrode: Mechanism and Potential Applications, *J. Mater. Chem. A*, 2020, **8**(40), 20979–20986, DOI: 10.1039/D0TA05656A.

55 S. H. Jung, K. Oh, Y. J. Nam, D. Y. Oh, P. Brüner, K. Kang and Y. S. Jung, Li_3BO_3–Li_2CO_3: Rationally Designed Buffering Phase for Sulfide All-Solid-State Li-Ion Batteries, *Chem. Mater.*, 2018, **30**(22), 8190–8200, DOI: 10.1021/acs.chemmater.8b03321.

56 S. Liu, H. Wu, L. Huang, M. Xiang, H. Liu and Y. Zhang, Synthesis of $Li_2Si_2O_5$-Coated $LiNi_{0.6}Co_{0.2}Mn_{0.2}O_2$ Cathode Materials with Enhanced High-Voltage Electrochemical Properties for Lithium-Ion Batteries, *J. Alloys Compd.*, 2016, **674**, 447–454, DOI: 10.1016/j.jallcom.2016.03.060.

57 A. Sakuda, A. Hayashi and M. Tatsumisago, Interfacial Observation between $LiCoO_2$ Electrode and Li_2S—P_2S_5 Solid Electrolytes of All-Solid-State Lithium Secondary Batteries Using Transmission Electron Microscopy, *Chem. Mater.*, 2010, **22**(3), 949–956, DOI: 10.1021/cm901819c.

58 Q. Zhang, W. Jiang, Z. Zhou, S. Wang, X. Guo, S. Zhao and G. Ma, Enhanced Electrochemical Performance of Li_4SiO_4-Coated $LiFePO_4$ Prepared by Sol–Gel Method and Microwave Heating, *Solid State Ionics*, 2012, **218**, 31–34, DOI: 10.1016/j.ssi.2012.05.006.

59 C. Zhang, L. Shen, H. Li, N. Ping and X. Zhang, Enhanced Electrochemical Properties of MgF_2 and C Co-Coated $Li_3V_2(PO_4)_3$ Composite for Li-Ion Batteries, *J. Electroanal. Chem.*, 2016, **762**, 1–6, DOI: 10.1016/j.jelechem.2015.12.022.

60 S.-X. Zhao, H. Ding, Y.-C. Wang, B.-H. Li and C.-W. Nan, Improving Rate Performance of $LiFePO_4$ Cathode Materials by Hybrid Coating of Nano-Li_3PO_4 and Carbon, *J. Alloys Compd.*, 2013, **566**, 206–211, DOI: 10.1016/j.jallcom.2013.03.041.

